Self-Optimizing Local Voltage Control of SOP in Active Distribution Networks Based on Lift-Dimension Mapping Linearization

Jingrong Su, *Graduate Student Member*, *IEEE*, Haoran Ji, *Senior Member*, *IEEE*, Peng Li*, *Senior Member*, *IEEE*, Hao Yu, *Senior Member*, *IEEE*, Jiancheng Yu, Jinli Zhao, *Member*, *IEEE*, Guanyu Song, *Senior Member*, *IEEE*, Jianzhong Wu, *Fellow*, *IEEE*, and Chengshan Wang, *Senior Member*, *IEEE*

***Abstract*—The high penetration of distributed generators (DGs) deteriorates the voltage violations in active distribution networks (ADNs). Owing to the flexible adjustment capacity, the local power regulation provided by soft open point (SOP) presents a promising solution for eliminating voltage violations in ADNs. A data-driven local control method can fully excavate the potential logic from operational data without requiring precious network parameters. However, the training data may be insufficient in practical applications. In this paper, a self-optimizing local voltage control method for SOP is proposed to achieve adaptive control in label-poor conditions. First, a SOP local control model is constructed based on lift-dimension mapping linearization (LDML), which portrays the complex relationship between ADN states and SOP control strategies. Subsequently, a self-optimizing guidance mechanism is established to obtain the label data of SOP control strategy, which provides a large number of training samples for the local control model. Finally, the effectiveness of the proposed method is validated using a practical distribution network with a four-terminal SOP. Results demonstrate that efficient control strategies can be determined based on local state measurements. A rapid response to DG fluctuations can be achieved while enhancing the adaptability to variations in practical operations.**

***Index Terms*—active distribution networks (ADNs), soft open point (SOP), distributed generators (DGs), self-optimizing voltage control, lift-dimension mapping linearization (LDML).**

NOMENCLATURE

Indices

i	Indices of measurements numbers, from 1 to N_{n}
k	Indices of iteration numbers, from 1 to N_{k}
l	Indices of lift dimensions at the SOP local control model, from 1 to N_{L}
m	Indices of update interval
n	Indices of control interval
t	Indices of time, from 1 to T

Variable

$\boldsymbol{A}$	Voltage fitting matrix
$\boldsymbol{B}$	State-strategy linear mapping matrix
$\boldsymbol{C}$	Lift-dimension basis matrix
$\boldsymbol{c}_l$	The lth basis vector in the lift-dimension basis matrix
$\boldsymbol{P}_t^{\mathrm{DG}}, \boldsymbol{Q}_t^{\mathrm{DG}}$	Real-time active/reactive power injection by DG at period t
$\boldsymbol{P}_t^{\mathrm{Load}}, \boldsymbol{Q}_t^{\mathrm{Load}}$	Real-time active/reactive power injection by load at period t
$\boldsymbol{P}_t^{\mathrm{Node}}, \boldsymbol{Q}_t^{\mathrm{Node}}$	Real-time nodal active/reactive power injection at period t
$\boldsymbol{P}_t^{\mathrm{SOP}}, \boldsymbol{Q}_t^{\mathrm{SOP}}$	Real-time active/reactive power injection by SOP at period t
$\boldsymbol{P}_t^{\mathrm{State}}, \boldsymbol{Q}_t^{\mathrm{State}}$	Real-time operational states at period t
$\boldsymbol{W}, \boldsymbol{V}$	Training dataset of voltage fitting component
$\boldsymbol{v}_t^{\mathrm{hist}}$	Measured nodal voltage at period t
$\boldsymbol{v}_t^{(k)}$	Estimated nodal voltage of the kth iteration at period t
$\Delta\boldsymbol{v}_t^{(k)}$	Estimated nodal voltage variation of the kth iteration at period t
$\boldsymbol{w}_t^{\mathrm{hist}}$	Measured nodal power injection at period t
$\boldsymbol{w}_t^{(k)}$	Estimated nodal power injection associated with optimized SOP control strategy of the kth iteration at period t
$\boldsymbol{x}_t, \boldsymbol{y}_t$	Real-time input/output of the state-strategy linear mapping matrix at period t
$\boldsymbol{X}, \boldsymbol{Y}$	Training dataset of the state-strategy linear mapping matrix
$\boldsymbol{x}$	Operational state of ADN
$\boldsymbol{x}^{\mathrm{L}}$	Lift-dimension input variable
$\boldsymbol{x}_t^{\mathrm{hist}}$	Historical operational state at period t
$\boldsymbol{y}$	SOP control strategy
$\boldsymbol{y}_t^{\mathrm{hist}}$	Label data of SOP control strategy associated with operational state at period t
$\boldsymbol{y}_t^{(k)}$	Optimized SOP control strategy of the k th iteration at period t
$\Delta\boldsymbol{y}_t^{(k)}$	Strategy adjustment value of the kth iteration at period t
$\boldsymbol{\psi}$	Lift-dimension augmented vector

This work was supported by the National Natural Science Foundation of China (52277117, U24B6010) and Natural Science Foundation of Tianjin (No. 24JCYBJC01250).

J. Su, H. Ji, P. Li, H. Yu, J. Zhao, G. Song, and C. Wang are with the State Key Laboratory of Intelligent Power Distribution Equipment and System, Tianjin University, Tianjin 300072, China (email: lip@tju.edu.cn). (Corresponding author: Peng Li.)

J. Yu is with the State Grid Tianjin Electric Power Company, Tianjin, China (email: yujiancheng@126.com).

J. Wu is with the Institute of Energy, School of Engineering, Cardiff University, Cardiff CF24 3AA, U.K. (email: wuj5@cardiff.ac.uk).

$\hat{\boldsymbol{\Phi}}_t^{(k)}$	Pseudo partial derivative of the kth iteration at period t
Parameter	
N_{k}	Total number of iterations
N_{l}	Total number of lift dimensions at the SOP local control model
N_{n}	Total number of critical nodes
T	Total optimization horizon of local voltage control method
T_{c}	Control horizon of SOP local control model
T_{s}	Update horizon of voltage fitting matrix and state-strategy linear mapping matrix
v^{ref}	Voltage reference of critical nodes
η, μ, ρ, λ	Adjustment parameters of label data generation
ε	Predefined tolerance in label data generation

I. Introduction

In recent years, distributed generators (DGs) have been increasingly integrated into active distribution networks (ADNs) [1], resulting in frequent voltage fluctuations and violations [2]. With the rapid development of power electronic technology, flexible devices represented by soft open points (SOPs) have been widely employed in the ADN [3]. Owing to the adjustable characteristics of power regulation capacity [4], SOP can effectively eliminate voltage violations in ADNs, which has become a viable solution for overcoming voltage-related issues.

Based on the accurate network parameters and global information, centralized methods typically construct complex optimization problems to obtain the optimal voltage control performance [5]. The authors in [6] proposed a day-ahead optimal control method for SOP with a chance-constrained optimization framework. In [7], a robust mixed-integer convex model was constructed to realize an optimal control for integrated energy storage and SOP in the day-ahead stage. A centralized model predictive voltage control method was presented in [8] to regulate the node voltage within the targeted limit. Owing to the large computational and communication overhead, the centralized voltage control method is typically realized over a long timespan. This may not help in fully utilizing the rapid response capacity of SOP to address the real-time uncertainties caused by the high penetration of DGs.

Local control presents a fast response to frequent state variations based only on local measurements when compared with centralized control [9]. Local control manages voltage regulation with fewer communication burdens and presents considerable potential for fast and flexible adjustment of SOP [10]. In [11], an improved hierarchical volt/var and volt/watt control method was proposed with a dual-balancing rule, determining the outputs of SOP and DGs using optimized droop curves. In [12], a real-time coordinated voltage control method was proposed with precise ADN parameters to determine the optimal operation of SOP and electric vehicles. The authors in [13] proposed a local voltage control method based on the lifted linear decision rule, which provides more flexible control strategies for handling frequent voltage fluctuations in ADNs. Local control methods based on accurate network parameters can achieve good voltage control performance. However, the difficulty in obtaining accurate parameters presents significant challenges for the practical application of physical-model-based control methods.

Owing to the widespread deployment of smart measurement devices, large amounts of operational data can be obtained from ADNs [14], which serve as a foundation for data-driven control methods. Data-driven methods can directly utilize the operational data to represent and analyze the complex nonlinear relationship between the inputs and outputs [15]. Thus, a more efficient and intelligent operation control of SOP can be achieved without requiring accurate physical parameters [16].

There are two types of data-driven methods namely iteration-based and machine learning-based methods. Iteration-based methods depend on real-time measurement feedback to realize adaptive adjustments of the control strategies [17]. The authors in [18] presented a data-driven var-voltage sequential control method, which incrementally updated strategies along the operation trajectory until it approached a near-optimal condition. A decentralized gradient descent-based algorithm was proposed in [19] to achieve online optimal voltage feedback control. In [20], a real-time control framework with an iterative structure was proposed for SOP, effectively adapting to changes in the operational environment. However, the step-by-step control required for these methods inevitably involves iterative interactions with a practical ADN, which may cause continuous disturbances to normal operations.

Conversely, machine-learning-based methods utilize historical data to train artificial neural networks, which can capture hidden operational features to simulate an actual ADN [21]. These methods can eliminate the need for real-time interaction with a practical ADN by using the artificial neural networks. An improved deep reinforcement learning algorithm with a projection layer was presented in [22], which addressed DG uncertainty and ensured the safe operation without voltage security violations. In [23], a voltage control framework was proposed by integrating the deep reinforcement learning method and the physics-informed representation network. A full-model-free adaptive graph deep deterministic policy gradient model was established in [24] for SOP voltage control, alleviating the need for accurate and timely network parameters. In [25], an edge intelligence-based control method was proposed for SOP with energy storage system, which can effectively enhance both the spatial and temporal flexibility in the ADN. However, the model training process depends on large amounts of historical data, which may be time-consuming. Furthermore, the model may not be adaptable to environmental variations, necessitating retraining to effectively accommodate new network conditions, such as changes in topology. Insufficient training data under such varying conditions may hinder the control performance of machine-learning-based methods, potentially leading to failure.

In this paper, a self-optimizing local voltage control method based on lift-dimension mapping linearization (LDML) is proposed to realize the active voltage support of SOP under label-poor conditions. The main contributions of this paper are

summarized as follows.

1) A data-driven local voltage control model is constructed for SOP without requiring accurate network parameters. By using LDML, the mapping between the operational states and SOP control strategies is excavated to establish the local control model. Based on the local state measurements, the voltage control strategy of SOP is rapidly determined by the local control model, which can respond to DG fluctuations during real-time operation.

2) A self-optimizing guidance mechanism is established to generate abundant label data for training the SOP local control model. By utilizing accumulated operational states, optimized SOP control strategies are derived, which then serve as label data for the control model. The self-optimizing training can be realized under label-poor conditions while mitigating the dependence on the historical label data.

The remainder of this paper is organized as follows. In Section II, an LDML-based data-driven method is introduced to describe the state-strategy relationship and construct the local control model of SOP. Section III presents the design of a self-optimizing guidance mechanism to obtain the label data for the SOP control strategy. In Section IV, case studies are conducted on a pilot distribution network with a four-terminal SOP. Finally, Section V presents the conclusions.

II. State-Strategy Relationship Description Based on Lift-dimension Mapping Linearization

The relationship between the operational states and SOP strategies in an ADN is characterized by high complexity and nonlinearity. It may be time-consuming to solve complex optimization problems established based on accurate physical parameters, making it difficult to suppress voltage fluctuations in real time. In this section, a data-driven method for SOP is proposed based on LDML. The proposed method enables flexible SOP adjustment corresponding to the current states of the ADN, which can realize a fast voltage control.

A. LDML-based local control model for SOP

The operational state of the ADN provides the basis for determining the SOP control strategy, which exhibits a complex nonlinear relationship, as expressed in Eq. (1).

$$\boldsymbol{y} = f(\boldsymbol{x}) \tag{1}$$

The operational state $\boldsymbol{x}$ is obtained from the sum of the DG outputs and load demands, as shown in (2).

$$\boldsymbol{x} = \begin{bmatrix} \boldsymbol{P}^{\mathrm{State}} \\ \boldsymbol{Q}^{\mathrm{State}} \end{bmatrix} = \begin{bmatrix} \boldsymbol{P}^{\mathrm{DG}} + \boldsymbol{P}^{\mathrm{Load}} \\ \boldsymbol{Q}^{\mathrm{DG}} + \boldsymbol{Q}^{\mathrm{Load}} \end{bmatrix} \tag{2}$$

The control strategy $\boldsymbol{y}$ comprises the active power transfer $\boldsymbol{P}^{\mathrm{SOP}}$ and reactive power output $\boldsymbol{Q}^{\mathrm{SOP}}$ of the SOP, as shown in Eq. (3).

$$\boldsymbol{y} = [\boldsymbol{P}^{\mathrm{SOP}} \quad \boldsymbol{Q}^{\mathrm{SOP}}]^{\mathrm{T}} \tag{3}$$

Owing to the difficulty in fitting the complex nonlinear relationships in (1), a data-driven model is constructed for the local voltage control of SOP based on the Koopman operator [26]. The Koopman operator presents the concept of lift dimension mapping and provides a global linear representation of the nonlinearity. Specifically, a low-dimensional nonlinear relationship can be converted into a high-dimensional linear formulation by expanding the original nonlinear features. Thus, the dynamic and nonlinear characteristics of (1) can be captured using a Koopman-based linear model. The lift-dimension mapping linearization can be used to excavate the hidden logic between the operational states and SOP control strategies into the linear mapping matrix $\boldsymbol{B}$. The equivalent linear model is expressed as follows.

$$\boldsymbol{y} = \boldsymbol{B}\boldsymbol{x}^{\mathrm{L}} = \boldsymbol{B}\begin{bmatrix} \boldsymbol{x} \\ \boldsymbol{\psi}(\boldsymbol{x}) \end{bmatrix} \tag{4}$$

where $\boldsymbol{x}^{\mathrm{L}}$ represents the lift-dimension augment, which includes the original state measurements $\boldsymbol{x}$ and the introduced nonlinear features $\boldsymbol{\psi}(\boldsymbol{x})$.

B. Data-driven solution for SOP local control model

The core of the proposed linear control model in (4) is the state-strategy linear mapping matrix $\boldsymbol{B}$, which can be obtained by a data-driven approach. The training dataset $\boldsymbol{Z}$ is formulated by the input matrix $\boldsymbol{X}$ and strategy matrix $\boldsymbol{Y}$. The mathematical structure of the training dataset can be described as follows.

$$\begin{gathered} \boldsymbol{Z} = \{\boldsymbol{X}, \boldsymbol{Y}\} \\ \boldsymbol{X} = \begin{bmatrix} \boldsymbol{x}_1^{\mathrm{hist}} & \cdots & \boldsymbol{x}_t^{\mathrm{hist}} & \cdots & \boldsymbol{x}_{mT_{\mathrm{s}}}^{\mathrm{hist}} \end{bmatrix} \\ \boldsymbol{Y} = \begin{bmatrix} \boldsymbol{y}_1^{\mathrm{hist}} & \cdots & \boldsymbol{y}_t^{\mathrm{hist}} & \cdots & \boldsymbol{y}_{mT_{\mathrm{s}}}^{\mathrm{hist}} \end{bmatrix} \end{gathered} \tag{5}$$

If the original inputs in (2) are lifted into an infinite-dimensional Hilbert state space, the non-linearity can be fully reconstructed by a linear model without any loss of accuracy. This method may be impractical due to overfitting, computational complexity, and algorithm adaptation. In fact, partial accuracy can be sacrificed for operational feasibility. Therefore, the Hilbert state space can be approximated in a finite-dimensional manner. This can be achieved by introducing a finite set of nonlinear features that are generated by an appropriately selected lift-dimension augmented function. In this section, the polyharmonic function is selected as the lift-dimension augmented function, as shown in (6).

$$f^{\mathrm{Lift}}(\boldsymbol{x} - \boldsymbol{c}) = \|\boldsymbol{x} - \boldsymbol{c}\|_2 \log\|\boldsymbol{x} - \boldsymbol{c}\|_2 \tag{6}$$

When the dimensionality is increased by N_{l} dimensions, $\boldsymbol{\psi}(\boldsymbol{x})$ can be described as follows.

$$\begin{gathered} \boldsymbol{\psi}(\boldsymbol{x}_t^{\mathrm{hist}}) = \begin{bmatrix} \psi_1(\boldsymbol{x}_t^{\mathrm{hist}}) & \cdots & \psi_l(\boldsymbol{x}_t^{\mathrm{hist}}) & \cdots & \psi_{N_{\mathrm{l}}}(\boldsymbol{x}_t^{\mathrm{hist}}) \end{bmatrix}^{\mathrm{T}} \\ \psi_l(\boldsymbol{x}_t^{\mathrm{hist}}) = f^{\mathrm{Lift}}(\boldsymbol{x}_t^{\mathrm{hist}} - \boldsymbol{c}_l) \\ \boldsymbol{C} = \begin{bmatrix} \boldsymbol{c}_1 \\ \vdots \\ \boldsymbol{c}_l \\ \vdots \\ \boldsymbol{c}_{N_{\mathrm{l}}} \end{bmatrix} = \begin{bmatrix} c_{1,1} & c_{1,2} & \cdots & c_{1,2N_{\mathrm{n}}} \\ \vdots & \vdots & & \vdots \\ c_{l,1} & c_{l,2} & \cdots & c_{l,2N_{\mathrm{n}}} \\ \vdots & \vdots & & \vdots \\ c_{N_{\mathrm{l}},1} & c_{N_{\mathrm{l}},2} & \cdots & c_{N_{\mathrm{l}},2N_{\mathrm{n}}} \end{bmatrix} \end{gathered} \tag{7}$$

where $\boldsymbol{c}_l$ denotes the lth basis vector related to ψ_l, whose magnitude should remain consistent with the input $\boldsymbol{x}$.

After constructing the training dataset, the linear mapping matrix $\boldsymbol{B}$ in (4) can be determined using the least-squares method, as shown in (8). This process is both time-efficient and

computationally lightweight, enabling rapid model training.

$$\boldsymbol{B} = \boldsymbol{Y}(\boldsymbol{X}^{\mathrm{L}})^{\mathrm{T}}[\boldsymbol{X}^{\mathrm{L}}(\boldsymbol{X}^{\mathrm{L}})^{\mathrm{T}}]^{\dagger} \tag{8}$$

where $[\cdot]^{\dagger}$ denotes the Moore-Penrose inverse of the matrix.

Thus, the local voltage control model can be constructed in a data-driven manner. The linear representation offers a rapid formulation in determining the SOP control strategy. The lift dimension input $\boldsymbol{x}_t^{\mathrm{L}}$ is first generated based on real-time state measurements, as shown in (9). The SOP control strategy $\boldsymbol{y}_t$ can then be obtained through a simple matrix calculation, making it particularly suitable for real-time voltage regulation.

$$\boldsymbol{y}_t = \begin{bmatrix} \boldsymbol{P}_t^{\mathrm{SOP}} \\ \boldsymbol{Q}_t^{\mathrm{SOP}} \end{bmatrix} = \boldsymbol{B}\boldsymbol{x}_t^{\mathrm{L}} = \boldsymbol{B}\begin{bmatrix} \boldsymbol{P}_t^{\mathrm{State}} \\ \boldsymbol{Q}_t^{\mathrm{State}} \\ \boldsymbol{\psi}(\boldsymbol{P}_t^{\mathrm{State}}) \\ \boldsymbol{\psi}(\boldsymbol{Q}_t^{\mathrm{State}}) \end{bmatrix} \tag{9}$$
$$t = mT_{\mathrm{s}} + 1, \cdots, (m+1)T_{\mathrm{s}}$$

***Note that*:** The model construction and the strategy formulation only rely on the measurements from critical nodes, which include the grid-connected nodes of the DGs and SOP, nodes with key loads, and nodes with three or more branches.

In summary, the complex nonlinear relationship between the operational states and SOP control strategies can be extracted into a linear mapping matrix based on lift-dimension mapping linearization. Subsequently, a SOP local control model is constructed using the state-strategy mapping matrix, thereby satisfying the demand for real-time voltage regulation under weak network parameters.

III. Self-optimizing Guidance Mechanism for SOP Local Control Strategy

The training of the SOP local control model depends on large amounts of high-quality data. However, the optimized SOP control strategies may not be available for practical operations, limiting the effectiveness of the proposed data-driven method. In this section, a self-optimizing guidance mechanism is presented to obtain the training label data. The optimal label data of the control strategy can be generated based on the accumulated operational states, thereby providing abundant label data for the SOP local control model.

A. Self-optimizing guidance mechanism

The proposed mechanism includes two parts: the self-optimizing generation of label data and dynamic fitting of voltages in the ADN, as shown in Fig. 1.

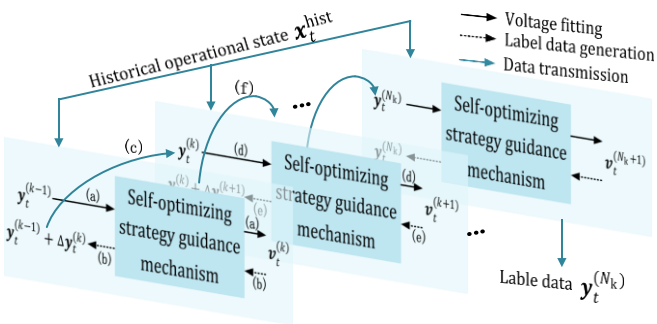

Fig. 1. Iterative generation of the self-optimizing SOP label data

The self-optimizing guidance mechanism generates the label data in an iterative form. Considering the kth iteration as an example, the interactive process between the two parts can be described as follows:

(a) In the voltage fitting component, the SOP control strategy $\boldsymbol{y}_t^{(k-1)}$, which is generated in the $k-1$ th iteration, is considered as the input. After $\boldsymbol{y}_t^{(k-1)}$ is fed into this part, the voltage response $\boldsymbol{v}_t^{(k)}$ can be obtained at the kth iteration.

(b) The voltage information $\boldsymbol{v}_t^{(k)}$ is transferred as the input for label data generation. The adjustment value of the SOP control strategy $\Delta\boldsymbol{y}_t^{(k)}$ is obtained as the corresponding output in this step.

(c) The input control strategy $\boldsymbol{y}_t^{(k-1)}$ and adjustment value $\Delta\boldsymbol{y}_t^{(k)}$ are then added to obtain the control strategy of the kth iteration, $\boldsymbol{y}_t^{(k)}$.

1) Self-optimizing generation of label data

In this subsection, a dynamic linearization framework of the ADN is established to achieve the self-optimizing generation of label data. The sensitivity relationship between the voltage control objective and SOP control strategy can be expressed by a pseudo partial derivative, which can be expressed as follows.

$$\begin{aligned} \Delta\boldsymbol{v}_t^{(k+1)} &= \hat{\boldsymbol{\Phi}}_t^{(k)}\Delta\boldsymbol{y}_t^{(k)} \\ \Delta\boldsymbol{v}_t^{(k+1)} &= \boldsymbol{v}_t^{(k+1)} - \boldsymbol{v}_t^{(k)} \\ \Delta\boldsymbol{y}_t^{(k)} &= \boldsymbol{y}_t^{(k)} - \boldsymbol{y}_t^{(k-1)} \end{aligned} \tag{10}$$

The criterion functions of the sensitivity and SOP control strategy are constructed as follows. μ and λ represent adjustable parameters with positive values, which are introduced to limit the variations of the pseudo partial derivative and the control strategy, respectively.

$$\begin{aligned} J\left(\hat{\boldsymbol{\Phi}}_t^{(k)}\right) = &\left\|\boldsymbol{v}_t^{(k)} - \boldsymbol{v}_t^{(k-1)} - \hat{\boldsymbol{\Phi}}_t^{(k)}\Delta\boldsymbol{y}_t^{(k-1)}\right\|_2^2 \\ &+\mu\left\|\hat{\boldsymbol{\Phi}}_t^{(k)} - \hat{\boldsymbol{\Phi}}_t^{(k-1)}\right\|_2^2 \end{aligned} \tag{11}$$

$$J(\boldsymbol{y}_t^{(k)}) = \left\|\boldsymbol{v}^{\mathrm{ref}} - \boldsymbol{v}_t^{(k+1)}\right\|_2^2 + \lambda\left\|\boldsymbol{y}_t^{(k)} - \boldsymbol{y}_t^{(k-1)}\right\|_2^2 \tag{12}$$

The first calculation term in (11) minimizes the tracking errors between the fitting and actual voltage, whereas the second term constrains the variation of the pseudo partial derivative to reduce the sensitivity of inaccurate or noisy data. As for the control strategy, the criterion function (12) balances the optimization of the voltage control objective and the smoothness of the control strategy. The minimization of the criterion functions yields the following iterative forms.

$$\hat{\boldsymbol{\Phi}}_t^{(k)} = \hat{\boldsymbol{\Phi}}_t^{(k-1)} + \frac{\eta\Delta\boldsymbol{y}_t^{(k-1)}(\Delta\boldsymbol{v}_t^{(k)} - \hat{\boldsymbol{\Phi}}_t^{(k-1)}\Delta\boldsymbol{y}_t^{(k-1)})}{\mu + \left\|\Delta\boldsymbol{y}_t^{(k-1)}\right\|_2^2} \tag{13}$$

$$\boldsymbol{y}_t^{(k)} = \boldsymbol{y}_t^{(k-1)} + \frac{\rho(\hat{\boldsymbol{\Phi}}_t^{(k)})^{\mathrm{T}}(\boldsymbol{v}^{\mathrm{ref}} - \boldsymbol{v}_t^{(k)})}{\lambda + \left\|(\hat{\boldsymbol{\Phi}}_t^{(k)})^{\mathrm{T}}\right\|_F^2} \tag{14}$$

The computational core is to find the adjustment value of the pseudo partial derivative and the control strategy. Eqs. (13) and (14) can be rewritten into the following forms.

$$\widehat{\boldsymbol{\Phi}}_t^{(N_\mathrm{k})} = \widehat{\boldsymbol{\Phi}}_t^{(0)} + \sum_{k=1}^{N_\mathrm{k}} \frac{\eta \Delta \boldsymbol{y}_t^{(k-1)} (\Delta \boldsymbol{v}_t^{(k)} - \widehat{\boldsymbol{\Phi}}_t^{(k-1)} \Delta \boldsymbol{y}_t^{(k-1)})}{\mu + \left\| \Delta \boldsymbol{y}_t^{(k-1)} \right\|_2^2} \tag{15}$$

$$\boldsymbol{y}_t^{(N_\mathrm{k})} = \boldsymbol{y}_t^{(0)} + \sum_{k=1}^{N_\mathrm{k}} \frac{\rho (\widehat{\boldsymbol{\Phi}}_t^{(k)})^\mathrm{T} (\boldsymbol{v}^{\mathrm{ref}} - \boldsymbol{v}_t^{(k)})}{\lambda + \left\| (\widehat{\boldsymbol{\Phi}}_t^{(k)})^\mathrm{T} \right\|_F^2} \tag{16}$$

To ensure the convergence of the proposed iterative solution, $\eta \in (0,2]$ and $\rho \in (0,1]$. In each iteration, the sensitivity matrix is first updated using the optimized control strategy and corresponding voltage response, as shown in (15). Then, the adjustment of the SOP control strategy is determined based on the newest sensitivity matrix.

The iterations are terminated when the voltage deviation between two consecutive iterations is lower than the predefined tolerance ε. In this paper, ε is set as 1×10^{-4}. The specific criterion is expressed as follows.

$$\left\| \boldsymbol{v}_t^{(k+1)} - \boldsymbol{v}_t^{(k)} \right\|_\infty < \varepsilon \tag{17}$$

$\boldsymbol{y}_t^{(N_\mathrm{k})}$ denotes the expected label data for period t. The operational state and label data constitute the input-output training sample of the LDML-based control model, as shown in (18). The training samples are periodically supplemented into the entire training dataset $\boldsymbol{Z}$ in (5).

$$\begin{cases} \boldsymbol{x}_t^{\mathrm{hist}} = \boldsymbol{x}_t^{(N_\mathrm{k})} \\ \boldsymbol{y}_t^{\mathrm{hist}} = \boldsymbol{y}_t^{(N_\mathrm{k})} \end{cases}, t = (m-1)T_\mathrm{s}, \cdots, mT_\mathrm{s} \tag{18}$$

***Remark 1*:** The effectiveness of the proposed dynamic linearization framework in (10) and iterative forms in (13) and (14) are proven in [27]. Therefore, the optimality of the SOP control strategy can be effectively ensured to realize the self-optimizing generation of the label data.

2) Dynamic fitting of ADN voltage profile

The optimized SOP control strategy should be executed in the ADN to obtain voltage feedback at each iteration, which may cause sustained disturbances. Additionally, the operational state is changed after multiple iterations, making it difficult to determine the timing correspondence between the operational state and label data. To address these issues, a data-driven voltage fitting component is further constructed to provide voltage profiles under different power injection scenarios.

To obtain the voltage fitting component, a training set is built based on the accumulated operational measurements, as shown in (19). The nodal power injection of critical nodes is considered as the input $\boldsymbol{W}$, and the voltage is obtained as the output $\boldsymbol{V}$. The input comprises the DG outputs, load demands, and SOP control strategies.

$$\begin{cases} \boldsymbol{W} = \left[\boldsymbol{w}_1^{\mathrm{hist}} \quad \cdots \quad \boldsymbol{w}_t^{\mathrm{hist}} \quad \cdots \quad \boldsymbol{w}_{mT_\mathrm{s}}^{\mathrm{hist}} \right] \\ \boldsymbol{V} = \left[\boldsymbol{v}_1^{\mathrm{hist}} \quad \cdots \quad \boldsymbol{v}_t^{\mathrm{hist}} \quad \cdots \quad \boldsymbol{v}_{mT_\mathrm{s}}^{\mathrm{hist}} \right] \end{cases}$$

$$\begin{aligned} \boldsymbol{w}_t^{\mathrm{hist}} &= \boldsymbol{x}_t^{\mathrm{hist}} + \boldsymbol{y}_t^{\mathrm{hist}} = [\boldsymbol{P}_t^{\mathrm{Node}} \quad \boldsymbol{Q}_t^{\mathrm{Node}}]^\mathrm{T} \\ \boldsymbol{P}_t^{\mathrm{Node}} &= \boldsymbol{P}_t^{\mathrm{DG}} + \boldsymbol{P}_t^{\mathrm{Load}} + \boldsymbol{P}_t^{\mathrm{SOP}} \\ \boldsymbol{Q}_t^{\mathrm{Node}} &= \boldsymbol{Q}_t^{\mathrm{DG}} + \boldsymbol{Q}_t^{\mathrm{Load}} + \boldsymbol{Q}_t^{\mathrm{SOP}} \end{aligned} \tag{19}$$

Then, the voltage fitting component is established based on the power-voltage mapping linear matrix $\boldsymbol{A}$ as follows.

$$\begin{aligned} \boldsymbol{v}_t^{(k)} &= \boldsymbol{A} \begin{bmatrix} \boldsymbol{w}_t^{(k)} \\ \boldsymbol{\psi}(\boldsymbol{w}_t^{(k)}) \end{bmatrix} = \boldsymbol{A} \begin{bmatrix} \boldsymbol{x}_t^{(k)} + \boldsymbol{y}_t^{(k-1)} \\ \boldsymbol{\psi}(\boldsymbol{x}_t^{(k)} + \boldsymbol{y}_t^{(k-1)}) \end{bmatrix} \\ \boldsymbol{A} &= \boldsymbol{V}(\boldsymbol{W}^\mathrm{L})^\mathrm{T} [\boldsymbol{W}^\mathrm{L} (\boldsymbol{W}^\mathrm{L})^\mathrm{T}]^\dagger \end{aligned} \tag{20}$$

$$\boldsymbol{W}^\mathrm{L} = \begin{bmatrix} \boldsymbol{w}_1^{\mathrm{hist}} & \cdots & \boldsymbol{w}_t^{\mathrm{hist}} & \cdots & \boldsymbol{w}_{mT_\mathrm{s}}^{\mathrm{hist}} \\ \boldsymbol{\psi}(\boldsymbol{w}_1^{\mathrm{hist}}) & \cdots & \boldsymbol{\psi}(\boldsymbol{w}_t^{\mathrm{hist}}) & \cdots & \boldsymbol{\psi}(\boldsymbol{w}_{mT_\mathrm{s}}^{\mathrm{hist}}) \end{bmatrix}$$

Data-driven voltage fitting can help in preventing real-time interaction with a practical ADN. The operational state is assumed to remain unchanged during the entire iteration at period t, that is $\boldsymbol{x}_t^{(1)} = \boldsymbol{x}_t^{(N_\mathrm{k})} = \cdots = \boldsymbol{x}_t^{\mathrm{hist}}$. The same inputs indicate that the self-optimizing guidance mechanism operates under the same source-load condition, which ensures a clear correspondence between the generated label data and the operational state. The inputs at different time points are temporally independent. Eq. (20) can be transformed into the following description.

$$\boldsymbol{v}_t^{(k)} = \boldsymbol{A} \begin{bmatrix} \boldsymbol{x}_t^{\mathrm{hist}} + \boldsymbol{y}_t^{(k-1)} \\ \boldsymbol{\psi}(\boldsymbol{x}_t^{\mathrm{hist}} + \boldsymbol{y}_t^{(k-1)}) \end{bmatrix} \tag{21}$$

The voltage fitting component provides a voltage response to the optimized SOP control strategy, contributing to the adjustment of the strategy in the next iteration to achieve better voltage control performance.

In summary, the optimal label data of the SOP control strategy is iteratively generated based on the proposed self-optimizing guidance mechanism. The operational states and corresponding label data constitute the training dataset, supporting the self-optimizing training of the SOP local control model under label-poor conditions.

B. Implementation of the SOP local voltage control

To enhance adaptability to the complex environments, the data-driven model for the local control of SOP is regularly retrained and updated at each update horizon within the edge computing device deployed in the ADN. The real-time measurements of DG outputs, load demands, and nodal voltages are taken as inputs, while the SOP control strategies are taken as outputs. Fig. 2 depicts a detailed implementation of the self-optimizing control of SOP.

(a) The operational data of ADN are collected to build the training dataset for the voltage fitting component, where nodal power injections are considered as the inputs, and voltage measurements are obtained as the outputs. The voltage fitting component is then constructed based on the operational data collected from 0 to mT_s.

When $t \in [0, T_\mathrm{s}]$, no control strategy is implemented for SOP. The initial operational data of ADN are used to initialize the proposed SOP local control model. When $t \in [mT_\mathrm{s}, (m+1)T_\mathrm{s}], m = 1,2,\cdots,(T - T_\mathrm{s})/T_\mathrm{s}$, the local control model is retrained at period mT_s, which represents the beginning of the update horizon. Then, the SOP control strategy can be determined using the updated model.

(b) Based on the self-optimizing guidance mechanism, the

label data of SOP control strategy are generated by utilizing operational states accumulated during the previous update horizon $[(m-1)T_s, mT_s]$. The operational state of the ADN and corresponding control strategy comprise an input-output training sample for the SOP local control model. Training samples from $(m-1)T_s$ to mT_s are then added to the overall training dataset of the SOP local control model.

(c) The state-strategy linear mapping matrix is trained based on the updated dataset, which includes data from 0 to mT_s. Subsequently, the linear matrix is used to reconstruct the SOP local control model.

(d) After retraining the data-driven control model, the SOP control strategy is determined based on the real-time operational state of the ADN, thereby effectively addressing the voltage violation problem.

(e) The operational data are collected to update the training dataset for the voltage fitting component. Each update horizon contains T_s/T_c samples, which are processed as a data chunk rather than being fed individually into the voltage fitting component.

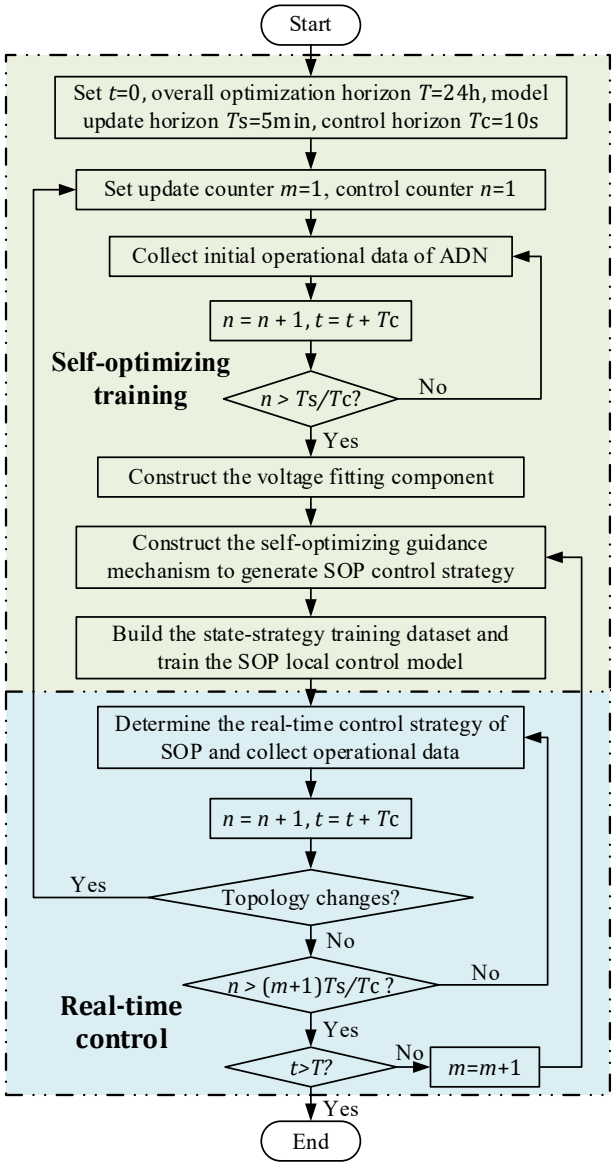

Fig. 2. Flowchart of the self-optimizing control of SOP

(f) If the network topology changes, it is assumed that no historical data are available, representing a label-poor condition. Thus, the proposed algorithm is restarted to adapt to the new topology. Two counters are reset to $m = 1$ and $n = 1$. Steps (a)-(c) are then executed to retrain the SOP local control model. Conversely, if the topology remains unchanged, steps (d) and (e) are executed until the operation is completed during the mth update horizon.

In the subsequent update horizons, steps (a)-(f) are repeated to support the self-optimizing update for the SOP local control model until the total optimization horizon T is reached.

***Note that*:** In this paper, the control horizon T_c and model update horizon T_s are set to 10 seconds and 5 minutes, respectively. The measurement sampling interval should be less than 10 seconds to ensure timely response, which can be realized by the supervisory control and data acquisition (SCADA) [28] or distribution-level phasor measurement unit (D-PMU) [29]. The control process can be completed within a few milliseconds, and the update process within a few seconds. Therefore, the control and update horizons are adjustable and flexible in practical applications.

IV. Case Studies and Analysis

In this section, a pilot distribution network constructed in Tianjin, China is selected to verify the effectiveness of the proposed method. The numerical experiments were conducted on a computer with an Intel(R) Core(TM) i7-12700 CPU processor running at 2.10 GHz and 32 GB of RAM.

A. Distribution networks with a four-terminal SOP

Fig. 3 depicts the structure of a practical distribution network with a four-terminal SOP. The rated voltage level is 10.5 kV. The active and reactive power of the load are 10.788 MW and 7.935 Mvar, respectively. The converters VSC1, VSC3, and VSC4 of the SOP are set to PQ control mode, enabling the regulation of active and reactive power flow on their connected feeders. The converter VSC2 operates in $U_{dc}Q$ control mode to stabilize the DC voltage [30].

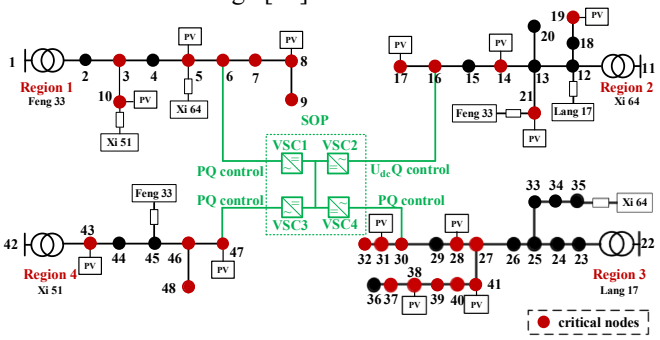

Fig. 3. Structure of practical distribution networks

13 groups of photovoltaics (PVs) are integrated into the system to consider the impact of the increasingly penetrating DGs. The active power of PVs reaches almost 60% of the peak load demand. Table I lists the detailed PV parameters. Fig. 4 and Fig. 5 depict the operation curves of the DG and load with a 10-second time interval. The capacity of each converter of the four-terminal SOP is set to 3.0 MVA. The minimum and

maximum limits of the voltage range are set to 0.95 p.u. and 1.05 p.u., respectively.

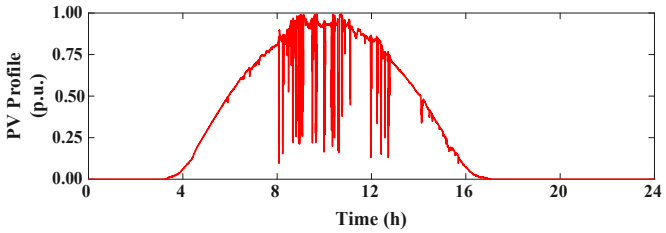

Fig. 4. Operation curve of the PV

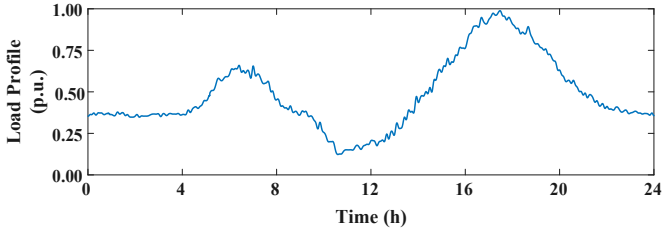

Fig. 5. Operation curve of the load

TABLE I
PARAMETERS OF PV INVERTER

Location	Capacity (kVA)	Location	Capacity (kVA)
5	200	28	400
8	200	31	400
10	400	38	1100
14	400	41	1100
17	600	43	200
19	400	47	400
21	600		

B. Evaluation metrics

The metrics used in the case study can be divided into two types: metrics for evaluating voltage control performance and metrics for assessing voltage fitting accuracy.

To evaluate the effectiveness of voltage optimization, the voltage deviation index (VDI) and the average deviation index (ADI) are introduced, which can be defined as follows.

$$\mathrm{VDI} = \sum_{t=1}^{T}\sum_{i=1}^{N_\mathrm{n}}\left|V^{\mathrm{ref}} - V_{i,t}\right| \tag{22}$$

$$\mathrm{ADI} = \frac{1}{T\times N_\mathrm{n}}\sum_{t=1}^{T}\sum_{i=1}^{N_\mathrm{n}}\left|\frac{V_{i,t}-V^{\mathrm{ref}}}{V^{\mathrm{ref}}}\right| \tag{23}$$

where $V_{i,t}$ denotes the voltage magnitude of node i at period t. V^{ref} denotes the reference voltage.

To further validate the optimality of the proposed method, the optimal rate index (ORI) is introduced to quantify the deviation between the proposed method and the theoretically optimal centralized method.

$$\mathrm{ORI} = \left(1 - \left|\frac{\Delta V_\mathrm{p}-\Delta V_\mathrm{c}}{\Delta V_\mathrm{c}-\Delta V_\mathrm{o}}\right|\right)\times 100\% \tag{24}$$

where ΔV_o, ΔV_p, and ΔV_c represent the voltage deviations of the initial operational state without any optimization, the proposed method, and the centralized optimal method, respectively.

The mean absolute error (MAE) is introduced to evaluate the accuracy of the voltage fitting component, which can be defined as follows.

$$\mathrm{MAE} = \frac{1}{N_\mathrm{F}\times N_\mathrm{n}}\sum_{f=1}^{N_\mathrm{F}}\sum_{i=1}^{N_\mathrm{n}}\left|\hat{V}_{i,f} - V_{i,f}\right| \tag{25}$$

where $\hat{V}_{i,f}$ and $V_{i,f}$ denote the predicted and true voltages, respectively. N_F denotes the total number of test datasets.

C. Optimization results analysis

1) Control effectiveness analysis

Four scenarios are adopted to validate the effectiveness of the proposed data-driven local voltage control method for SOP.

Scenario I: There is no control strategy conducted on SOP, which can obtain the initial operational data of the ADN.

Scenario II: The SOP control strategies are determined using the proposed lift-dimension mapping linearization method.

Scenario III: The SOP control strategies are regulated using a real-time centralized control method based on accurate network parameters, which can realize a theoretical optimization.

Scenario IV: The SOP control strategies are optimized using the model-free adaptive control (MFAC)-based voltage control method [20].

The optimization results for the four scenarios are listed in Table II.

TABLE II
COMPARISON OF CONTROL PERFORMANCE OF THE FOUR SCENARIOS

Scenario	Minimum voltage (p.u.)	Maximum voltage (p.u.)	VDI (p.u.)	ORI (%)
I	0.9220	1.0629	3625.1	/
II	0.9718	1.0440	1243.1	94.01
III	0.9660	1.0477	1091.4	100.00
IV	0.9524	1.0448	1507.3	83.59

The effectiveness of the proposed method is validated through a comparison of Scenarios I and II. The voltage deviations in the test system are severe in Scenario I, as shown in Fig. 6. Voltage overlimit occurs in Region 1 with heavy load demands and Region 3 with high-penetration DGs. In the initial operational conditions, the minimum and maximum voltage profiles are 0.9220 p.u. and 1.0629 p.u., respectively.

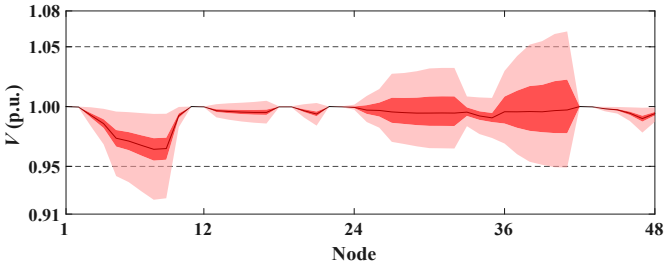

Fig. 6. Voltage control performance of Scenario I

Fig. 7 depicts the voltage control performance of Scenario II. A data-driven voltage control model of SOP is established based on real-time operational measurements. The proposed LDML-based method can effectively manage the frequent voltage deviations by utilizing the flexible power adjustment capacity of SOP. The voltage deviation under Scenario II is reduced by 65.71% when compared with Scenario I. The voltage range is narrowed to $[0.9718,1.0440]$, which is maintained at a secure operational level.

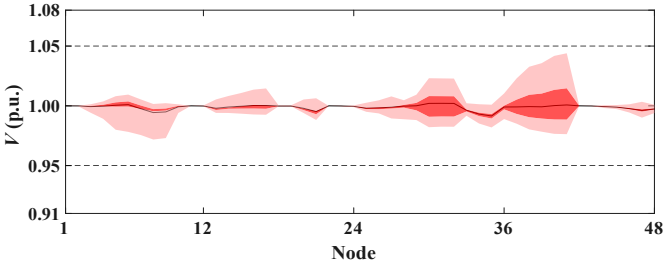

Fig. 7. Voltage control performance of Scenario II

The optimality of the proposed method is verified through a comparison of Scenarios II and III. Fig. 8 shows the voltage control performance of Scenario III. Owing to the heavy computational and communication burden, the centralized physical model-based method may be infeasible in practical operations. Therefore, it is only considered as a theoretically optimal result. The proposed LDML-based method determines the real-time control strategy based solely on the local measurements, thereby eliminating the dependence on accurate network parameters. The optimal rate of Scenario II is 94.01% and achieves approximate global optimization.

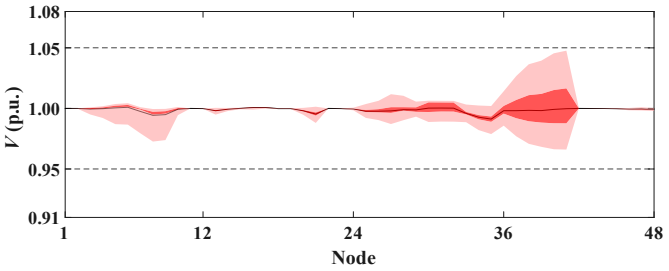

Fig. 8. Voltage control performance of Scenario III

The superiority of the proposed method is demonstrated through a comparison of Scenarios II and IV. The proposed method shows a better voltage control effect than the MFAC-based method, achieving a 17.5% reduction in VDI and a 12.4% improvement in ORI. Fig. 9 shows the voltage control performance of Scenario IV.

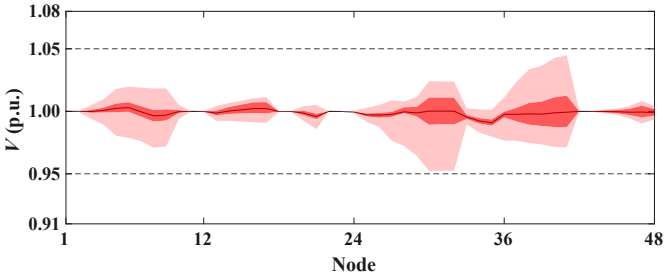

Fig. 9. Voltage control performance of Scenario IV

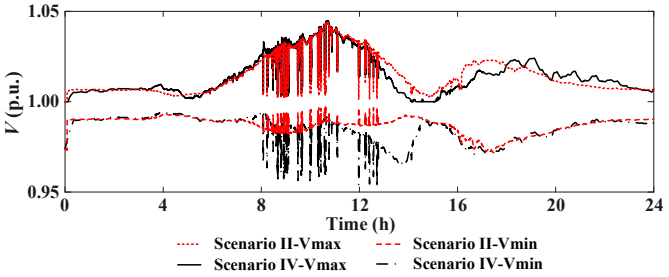

Fig. 10. Comparison of voltage profiles in Scenarios II and IV

As illustrated in Fig. 10, the maximum voltage of Scenario II and Scenario IV are generally close throughout the day, while significant differences are presented in the minimum voltage. When the DG outputs fluctuate dramatically during 8:00 to 15:00, the proposed method can mitigate the voltage deviations more effectively, highlighting its enhanced adaptability and regulation capability under volatile operational conditions.

2) Influence of the key measurements

The proposed method can be applied under the partially monitored condition, where the SOP local control model only needs key measurements from critical nodes in the ADN. When full measurements are available, data from all nodes can be used to achieve more efficient control. The control effect is analyzed in Table III.

TABLE III
COMPARISON OF CONTROL EFFECT UNDER KEY MEASUREMENTS

Scenario	Minimum voltage (p.u.)	Maximum voltage (p.u.)	VDI (p.u.)	ORI (%)
II. Fully monitored	0.9718	1.0402	1155.0	97.50
II. Partially monitored	0.9718	1.0440	1243.1	94.01

Numerical results indicate that the decrease in voltage control effect is minimal when only key measurements from critical nodes are used, demonstrating that the proposed method remains effective under the partially monitored condition.

3) Influence of the data availability

To reduce reliance on historical data, a self-optimizing guidance mechanism is established to generate abundant training labels from accumulated operational states during real-time operations. When sufficient data are available, the proposed method directly utilizes these data to train the SOP local control model, eliminating the need for the mechanism. Table IV presents the control performance under different levels of data availability.

TABLE IV
COMPARISON OF CONTROL PERFORMANCE UNDER DIFFERENT DATA AVAILABILITY

Scenario	Minimum voltage (p.u.)	Maximum voltage (p.u.)	VDI (p.u.)	ORI (%)
II. Insufficient data	0.9718	1.0440	1243.1	94.01
II. Sufficient data	0.9669	1.0399	1101.8	99.59

It can be seen from the numerical experiments that the VDI is reduced by 11.37% under sufficient data conditions, indicating a notable mitigation of voltage deviations. An ORI of 99.59% further demonstrates that the proposed method can achieve near-global optimization. Under insufficient data conditions, the ORI reaches 94.01%, confirming its ability to rapidly adapt to complex operational environments and maintain reliable performance without relying on historical data.

D. Update horizon analysis

When the state-strategy training samples are insufficient, the proposed method generates the training label data using the self-optimizing mechanism. The fitting accuracy of the nodal voltages will affect the generated label data. The construction of the voltage fitting component depends on real-time power

injections and voltage measurements. Frequent updates can accelerate the adjustment of the data-driven model, thereby preventing prolonged dependence on the outdated model with error accumulation. Thus, the update horizon is an important factor that affects the fitting accuracy and efficiency.

Table V lists the computational efficiency for the different update horizons. The convergence time represents the minimum time required to reach the expected fitting accuracy, where the desired value of MAE is set as 1×10^{-3}.

TABLE V
COMPUTATIONAL EFFICIENCY UNDER DIFFERENT UPDATE HORIZONS

Update horizon (min)	Calculation time (s)	Training time (s)	Convergence time (min)
1	5.60×10^{-5}	0.4346	12
5	4.59×10^{-5}	1.3450	50
10	4.40×10^{-5}	2.6738	560
15	5.13×10^{-5}	6.8600	585

Fig. 11 depicts the visual representation of this effect. The computation time is related to the scale of inputs, outputs, and lift dimensions, which are unaffected by the update horizon. Thus, when the update horizon changes, the computation time of the control strategy remains nearly constant. The training time grows significantly with a longer update horizon because the self-optimizing guidance mechanism needs to process more accumulated operational states of the previous update horizon.

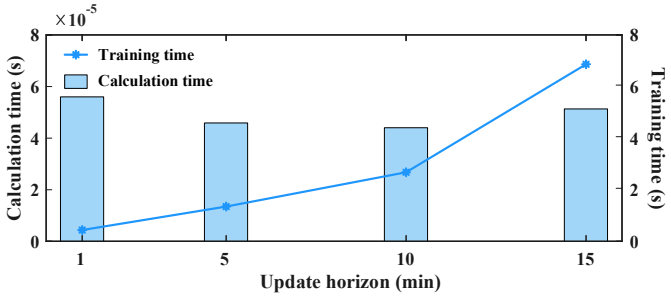

Fig. 11. Computational efficiency for different update horizons

In this paper, the control and update horizons are set to 10 seconds and 5 minutes, respectively. Numerical results indicate that the calculation time of the control strategy is 4.59×10^{-5} seconds while the training time is 1.3450 seconds, both of which are shorter than the setting values.

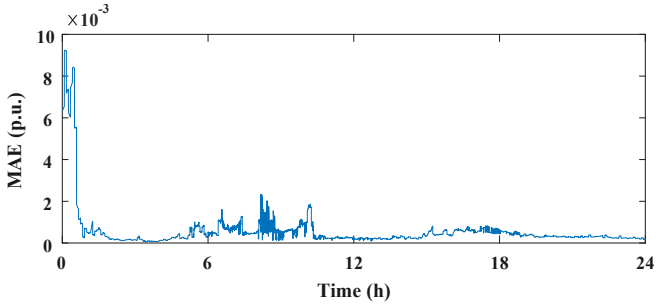

Fig. 12. Fitting error at the five-minute update horizon

Fig. 12 depicts the MAE distribution of the 5-minute update horizon. Starting with the proposed data-driven method in the absence of training samples, the expected fitting accuracy can be achieved within an operation time of 50 minutes. The DG outputs fluctuate drastically from 8:00-13:00, resulting in increased voltage fitting errors. The voltage fitting component is regularly updated based on the accumulated operational data, thereby enabling rapid adaptation to dynamic environments. Therefore, the fitting accuracy returns to the desired level after 10:30, rather than at the end of the DG fluctuations.

The update horizon affects both the accuracy of the voltage fitting component and the training of the SOP local control model, thereby influencing the control performance of the proposed voltage control strategy. Table VI presents the optimization results under different update horizons.

TABLE VI
CONTROL PERFORMANCE UNDER DIFFERENT UPDATE HORIZONS

Update horizon (min)	Minimum voltage (p.u.)	Maximum voltage (p.u.)	VDI (p.u.)
1	0.9720	1.0440	1236.2
5	0.9718	1.0440	1243.1
10	0.9518	1.0385	1548.4
15	0.9307	1.0404	1673.2

When the update horizon increases from 1 minute to 5 minutes, the voltage control performance remains almost the same. However, further increasing the update horizon reduces the responsiveness to dynamic changes in the ADN, resulting in considerable voltage deviations. Especially, when the update horizon is extended to 15 minutes, the minimum voltage drops below 0.95 p.u..

E. Adaptability to parameter settings

Scenarios II and IV both involve the selection of parameters ρ, η, μ, and λ. Parameter settings will influence the voltage control performance of the strategy. Thus, different parameters are set to analyze the parameter sensitivity. The parameter ρ is varied while the rest of parameters are kept constant, i.e., $\eta = 1$, $\mu = 1$, and $\lambda = 0.1$. Table VII lists the optimization results.

TABLE VII
OPTIMIZATION RESULTS OF DIFFERENT PARAMETERS AT NODE 30

Scenario	ρ	Minimum voltage (p.u.)	Maximum voltage (p.u.)	ADI (p.u.)
I	/	1.0009	1.0308	0.0276
II	0.1	0.9615	1.0300	0.0111
	0.5	0.9763	1.0300	0.0165
	1	0.9674	1.0300	0.0133
IV	0.1	0.9423	1.0299	0.0244
	0.5	0.9598	1.0299	0.0225
	1	0.9666	1.0299	0.0192

When the parameter ρ is set to 0.1, 0.5, and 1, the voltage deviations in Scenario II are reduced by 59.84%, 40.12%, and 51.81%, respectively. Furthermore, the reductions in Scenario IV are 11.47%, 18.28%, and 30.48%, respectively. The voltage control performance of the proposed method is significantly better than that of the MFAC-based method.

Fig. 13 and Fig. 14 show the control performance of Scenarios II and IV with different parameters, respectively. The minimum voltage in Scenario IV reduces to 0.9423 p.u. when ρ is set to 0.1, indicating that the MFAC-based method is

sensitive to the parameters. Since the parameter settings have a direct impact on the formulation of the SOP control strategy, inappropriate parameter choices may significantly degrade control performance and even lead to voltage violations. In contrast, Scenario II maintains the voltage within a desired range when the parameter ρ varies within the predefined range $(0,1]$. The proposed method mitigates the impact of parameters through a dual-layer isolation involving both data generation and model construction, thereby maintaining reliable control performance under different parameters.

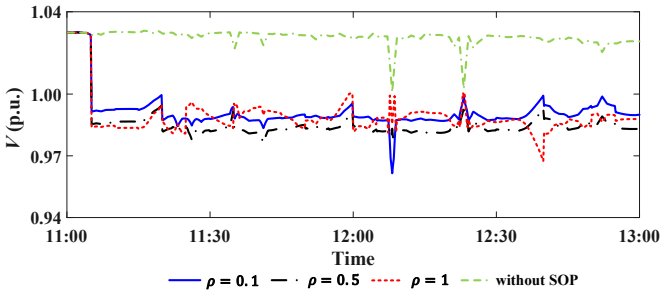

Fig. 13. Control performance in Scenario II with different parameter ρ

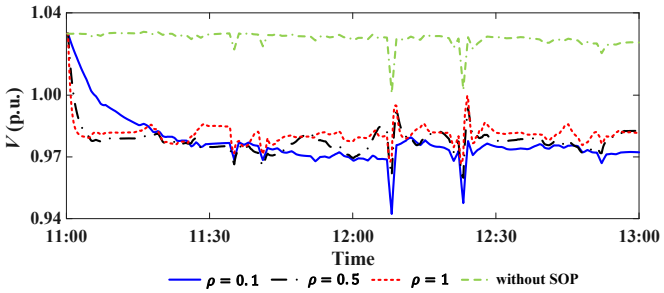

Fig. 14. Control performance in Scenario IV with different parameter ρ

The MFAC-based method inevitably affects normal operations due to the real-time interaction and feedback from the practical ADN. An uncertainty in the initial value may cause sustained disturbances during the dynamic iteration processes. The proposed method makes real-time decisions of the SOP control strategies without iterations. The one-step determination helps in effectively preventing negative impacts on daily operations.

F. Adaptability to DG fluctuations

The physical model-based centralized optimization method is primarily employed in the day-ahead stage due to the huge computational and communication burden. The SOP control strategies are optimized based on the source-load forecasting information. However, the strong uncertainty in the DG outputs presents significant challenges for such approaches. Scenario V is introduced to validate the adaptability of the proposed LDML-based method to DG fluctuations.

Scenario V: The SOP control strategies are regulated using a day-ahead centralized control method based on accurate network parameters [31].

Table VIII lists the overall control performance. The forecasting information over a long timescale varies significantly from the real-time fluctuations, which causes low matching of day-ahead strategies and deteriorates the control performance of Scenario V.

TABLE VIII
COMPARISON OF VOLTAGE CONTROL PERFORMANCE

Scenario	Minimum voltage (p.u.)	Maximum voltage (p.u.)	VDI (p.u.)
II	0.9718	1.0440	1243.1
V	0.9579	1.0483	1461.1

Fig. 15 depicts a comparison of the voltage control deviation at each node of Scenarios II and V. Nodes 38 and 41 are integrated with large-capacity DG units, making them significantly affected by DG fluctuations. Thus, the voltage deviations at these nodes are more pronounced.

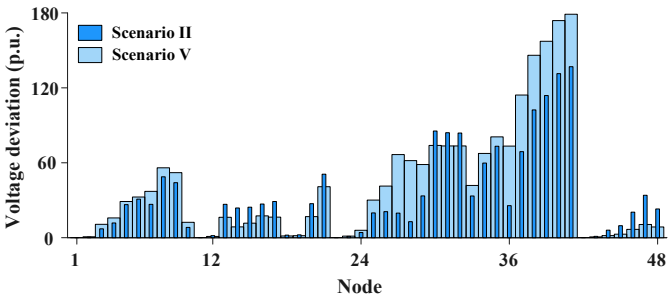

Fig. 15. Comparison of voltage deviations of Scenarios II and V

SOP control strategies in Scenario II are shown in Fig. 16 and Fig. 17. In response to the significant variations in DG outputs during 8:00 to 13:00, the active power transmission and reactive power output of SOP fluctuate dramatically. The active power of SOP is negative for high PV outputs, indicating that the active power in Region 3 is transferred to other heavy-load regions. The positive transfer of the active power and local compensation of the reactive power improve the distributions of the nodal voltages under heavy-load conditions. The proposed method fully exploits the accurate and rapid power regulation characteristics of SOP. It can mitigate the voltage fluctuations caused by highly penetrating DGs through power sharing between different regions.

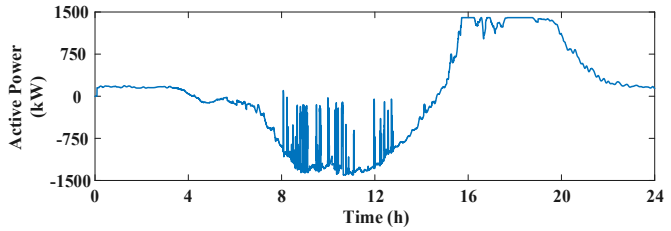

Fig. 16. Active power transmission of SOP in Region 3

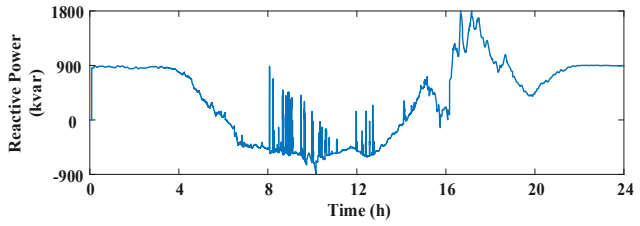

Fig. 17. Reactive power output of SOP in Region 3

Compared with centralized methods, the proposed method does not face computationally intensive optimization and convergence problems. The control process can be completed within a few milliseconds, meeting the real-time control requirements. In addition, the SOP local control model can be

retrained within a few seconds, supporting the frequent model updates and timely adaptation to frequent variations in the complex operational environments.

G. Adaptability to network topology changes

Topology reconfiguration modifies the network parameters and redistributes the power flow, causing a decline in the control effectiveness of the SOP strategy formulated under the original topology. Therefore, it is crucial to illustrate the adaptability of the proposed LDML-based method to varying network topologies.

It is assumed that a local topological change occurs at 11:00. As shown in Fig. 18, the branches between nodes 3 and 10, nodes 25 and 33 are disconnected. The tie switches between nodes 10 and 45, as well as nodes 12 and 35, are closed.

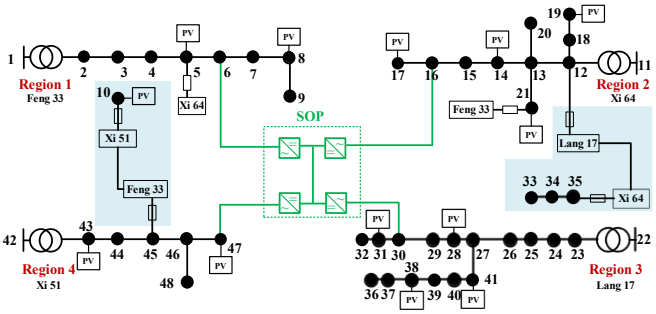

Fig. 18. Structure of distribution networks with topology reconfiguration

When network topology changes, the physical model cannot be updated in time, which negatively affects the effectiveness of the physical model-based control strategies. In contrast, as an iterative-based data-driven method, the MFAC-based method can dynamically adjust the SOP control strategies based on real-time feedback received from the ADN, which can adapt to frequently changing topologies. Table IX lists the optimization results under topology changes.

TABLE IX
OPTIMIZATION RESULTS UNDER TOPOLOGY CHANGES

Scenario	Minimum voltage (p.u.)	Maximum voltage (p.u.)	VDI (p.u.)	ADI (p.u.)
II	0.9649	1.0591	472.8	0.0039
IV	0.9463	1.0590	492.8	0.0041
V	0.9623	1.0453	587.4	0.0048

Numerical results demonstrate that the LDML-based method achieves superior voltage regulation performance. Although Scenario IV exhibits the VDI and ADI comparable to those of Scenario II, its minimum and maximum voltages exceed the desired operational range. Scenario V shows significantly higher VDI and ADI, suggesting that it fails to effectively adapt to the topology change due to the outdated physical model.

When the network topology changes, the proposed method collects the initial operational data during the first update horizon, serving as the foundation for generating label data and retraining the SOP local control model. During this short transition period, no control strategy is applied, causing the voltage in Scenario II to temporarily exceed 1.05 p.u.. As a result, voltage deviations of Scenario II are relatively large at the beginning, as shown in Fig. 19 and Fig. 20. However, the voltage is quickly regulated back to an acceptable range once the updated SOP local control model is deployed.

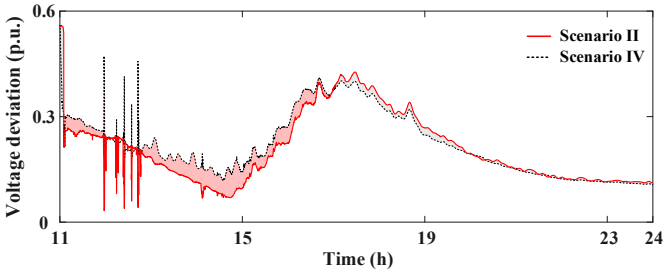

Fig. 19. Voltage deviation in Scenarios II and IV

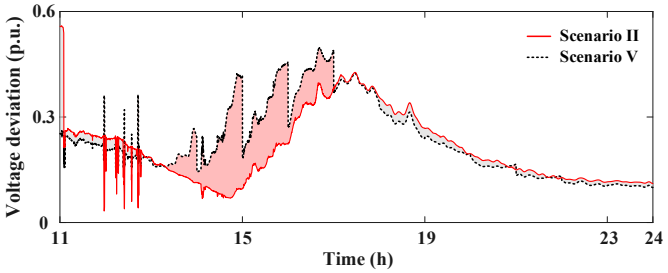

Fig. 20. Voltage deviation in Scenarios II and V

***Remark 2*:** Machine learning methods may require time-consuming training and struggle to adapt to changes in network topology, hindering the practicality of such methods. In contrast, the proposed LDML-based method continuously collects new operational data to enrich the training dataset and then updates the SOP local control model in a self-optimizing manner, enhancing the adaptability to topology changes and complex operational conditions.

V. CONCLUSIONS

In this paper, a self-optimizing local voltage control method for SOP is proposed to effectively mitigate the voltage violations caused by the high penetration of DGs. Leveraging a lift-dimension mapping linearization (LDML) framework, the proposed method formulates the linear mapping between the operational states and SOP control strategies, eliminating the need for accurate network parameters and improving feasibility for practical applications. Based on the linearized expression, the local control strategy of SOP can be derived within milliseconds, satisfying the real-time control requirements. Furthermore, a self-optimizing guidance mechanism is established to generate abundant label data from accumulated operational data, which supports efficient model training and reduces reliance on historical data. Simulation results validate that the proposed method fully exploits the flexible adjustment capacity of SOP to enhance the voltage control performance in ADNs while achieving approximate global optimization. Compared to conventional methods, the self-optimizing training enables rapid adaptation to complex operational environments and ensures reliable performance under label-poor conditions.

The future research of this paper can be carried out in the following directions. First, the proposed method updates the local control model in a fixed horizon, which cannot adaptively

adjust the update horizon according to voltage control performance. An event-triggered update mechanism can be designed to realize more flexible and efficient control of SOP. Second, the proposed method relies heavily on high-precision measurements. Addressing the measurement noise and bad data remains a key challenge for future research. Furthermore, other control devices in an ADN, such as on-load tap changers, capacitor banks, and energy storage systems, can be further developed. The coordination of multiple control devices should be investigated to fully utilize the available resources.

REFERENCES

[1] S. Li, Z. Li, X. Wan, *et al*. "Recent progress in flexible organic solar cells," *eScience*, vol. 3, no. 1, 100085, 2023.

[2] A. Tavakoli, S. Saha, M. Arif, *et al*. "Impacts of grid integration of solar PV and electric vehicle on grid stability, power quality and energy economics: a review," *IET Energy Syst. Int.*, vol. 2, no. 3, pp. 243-260, 2020.

[3] J. Jian, J. Zhao, H. Ji, *et al*. "Supply restoration of data centers in flexible distribution networks with spatial-temporal regulation," *IEEE Trans. Smart Grid*, vol. 15, no. 1, pp. 340-354, 2024.

[4] F. Sun, J. Ma, M. Yu, *et al*. "Optimized two-time scale robust dispatching method for the multi-terminal soft open point in unbalanced active distribution networks," *IEEE Trans. Sustain. Energy*, vol. 12, no. 1, pp. 587-598, 2021.

[5] J. Le, L. Zhao, C. Wang, et al. "Leader-follower optimal selection method for distributed control system in active distribution networks," CSEE J. Power Energy Syst., vol. 10, no. 1, pp. 314-323, 2024.

[6] C. Han, R. Rao, S. Cho. "Stochastic operation of multi-terminal soft open points in distribution networks with distributionally robust chance-constrained optimization," *IEEE Trans. Sustain. Energy*, vol. 16, no. 1, pp. 81-94, 2025.

[7] I. Sarantakos, M. Peker, N. Zografou-Barredo, *et al.* "A robust mixed-integer convex model for optimal scheduling of integrated energy storage—soft open point devices," *IEEE Trans. Smart Grid*, vol. 13, no. 5, pp. 4072-4087, 2022.

[8] S. Maharjan, A. Khambadkone, J. Peng. "Robust constrained model predictive voltage control in active distribution networks," *IEEE Trans. Sustain. Energy*, vol. 12, no. 1, pp. 400-411, 2021.

[9] C. Zhang, R. Xu, L. Yang. "Optimization of local voltage control with coordinating droop functions under high PV penetration," *IEEE Trans. Power Syst.*, vol. 39, no. 5, pp. 6776-6779, 2024.

[10] X. Jiang, Y. Zhou, W. Ming, *et al*. "An overview of soft open points in electricity distribution networks," *IEEE Trans. Smart Grid*, vol. 13, no. 3, pp. 1899-1910, 2022.

[11] Q. Hou, N. Dai, Y. Huang. "Voltage regulation enhanced hierarchical coordinated volt/var and volt/watt control for active distribution networks with soft open points," *IEEE Trans. Sustain. Energy*, vol. 15, no. 3, pp. 2021-2037, 2024.

[12] X. Yang, C. Xu, Y. Zhang, *et al*. "Real-time coordinated scheduling for ADNs with soft open points and charging stations," *IEEE Trans. Power Syst.*, vol. 36, no. 6, pp. 5486-5499, 2021.

[13] X. Xu, Y. Gao, H. Wang, *et al.* "Distributionally robust optimization of photovoltaic power with lifted linear decision rule for distribution system voltage regulation," *IEEE Trans. Sustain. Energy*, vol. 15, no. 2, pp. 758-772, 2024.

[14] Q. Wang, F. Li, Y. Tang, *et al*. "Integrating model-driven and data-driven methods for power system frequency stability assessment and control," *IEEE Trans. Power Syst.*, vol. 34, no. 6, pp. 4557-4568, 2019.

[15] N. Yang, J. Hao, Z. Li, *et al*. "Data-driven decision-making for SCUC: an improved deep learning approach based on sample coding and Seq2Seq technique," *Prot. Control Mod. Power Syst.*, vol. 10, no. 2, pp. 13-24, 2025.

[16] Z. Zhang, P. Li, H. Ji, *et al*. "Adaptive voltage control of inverter-based DG in active distribution networks with measurement-strategy mapping matrix," *IEEE Trans. Sustain. Energy*, vol. 16, no. 2, pp. 1238-1252, 2025.

[17] S. Li, W. Wu. "Adaptive voltage control to coordinate multiple PV inverters as a cluster," *IEEE Trans. Smart Grid*, vol. 15, no. 6, pp. 5526-5538, 2024.

[18] J. Zhang, Z. Chen, C. He, *et al*. "Data-driven-based optimization for power system var-voltage sequential control," *IEEE Trans. Ind. Inform.*, vol. 15, no. 4, pp. 2136-2145, 2019.

[19] Y. Guo, H. Gao, D. Wang, *et al*. "Online optimal feedback voltage control of wind farms: decentralized and asynchronous implementations," *IEEE Trans. Sustain. Energy*, vol. 12, no. 2, pp. 1489-1492, 2021.

[20] Y. Huo, P. Li, H. Ji, *et al*. "Data-driven adaptive operation of soft open points in active distribution networks," *IEEE Trans. Ind. Inform.*, vol. 17, no. 12, pp. 8230-8242, 2021.

[21] C. Jiang, Z. Lin, C. Liu, *et al*. "MADDPG-based active distribution network dynamic reconfiguration with renewable energy," *Prot. Control Mod. Power Syst.*, vol. 9, no. 6, pp. 143-155, 2024.

[22] M. Zhang, G. Guo, S. Magnusson, *et al.* "Data driven decentralized control of inverter based renewable energy sources using safe guaranteed multi-agent deep reinforcement learning," *IEEE Trans. Sustain. Energy*, vol. 15, no. 2, pp. 1288-1299, 2024.

[23] D. Cao, J. Zhao, J. Hu, *et al*. "Physics-informed graphical representation-enabled deep reinforcement learning for robust distribution system voltage control," *IEEE Trans. Smart Grid*, vol. 15, no. 1, pp. 233-246, 2024.

[24] H. Wu, Z. Xu, M. Wang, *et al*. "Full-model-free adaptive graph deep deterministic policy gradient model for multi-terminal soft open point voltage control in distribution systems," *J. Mod. Power Syst. Clean Energy*, vol. 12, no. 6, pp. 1893-1904, 2024.

[25] T. Qian, W. Ming, C. Shao, *et al*. "An edge intelligence-based framework for online scheduling of soft open points with energy storage," *IEEE Trans. Smart Grid*, vol. 15, no. 3, pp. 2934-2945, 2024.

[26] Z. Wang, J. Liu, X. Zhu, *et al*. "Model-free distributed voltage control for distribution networks based on state space mapping and super-linear feedback," *IEEE Trans. Power Syst.*, vol. 39, no. 5, pp. 6290-6304, 2024.

[27] Z. Hou, S. Jin. "Data-driven model-free adaptive control for a class of MIMO nonlinear discrete-time systems," *IEEE Trans. Neural Netw.*, vol. 22, no. 12, pp. 2173-2188, 2011.

[28] S. Huang, C. Lu, Y. Lo. "Evaluation of AMI and SCADA data synergy for distribution feeder modeling," *IEEE Trans. Smart Grid*, vol. 6, no. 4, pp. 1639-1647, 2015.

[29] J. Yang, H. Yu, P. Li, *et al*. "Real-time D-PMU data compression for edge computing devices in digital distribution networks," *IEEE Trans. Power Syst.*, vol. 39, no. 4, pp. 5712-5725, 2023.

[30] W. Liu, M. Fu, M. Yang, *et al*. "A bi-level interval robust optimization model for service restoration in flexible distribution networks," *IEEE Trans. Power Syst.*, vol. 36, no. 3, pp. 1843-1855, 2021.

[31] P. Li, H. Ji, C. Wang, *et al*. "Coordinated control method of voltage and reactive power for active distribution networks based on soft open point," *IEEE Trans. Sustain. Energy*, vol. 8, no. 4, pp. 1430-1442, 2017.

Jingrong Su (Graduate Student Member, IEEE) received the B.S. in electrical engineering from Tianjin University, Tianjin, China, in 2023.

She is currently pursuing the M.S. degrees in electrical engineering in Tianjin University. Her current research interests include optimal operation of active distribution networks.

Haoran Ji (Senior Member, IEEE) received the B.S. and Ph.D. degrees in electrical engineering from Tianjin University, Tianjin, China, in 2014 and 2019, respectively.

From 2019 to 2021, he was a Post-Doctoral Research with Tianjin University, where he is currently a Professor. He was supported by China National Post-Doctoral Program for Innovative Talents. His research interests include distributed generation systems and optimal operation of distribution networks.

Peng Li (Senior Member, IEEE) received the B.S. and Ph.D. degrees in electrical engineering from Tianjin University, Tianjin, China, in 2004 and 2010, respectively.

He is currently a Professor with the School of Electrical and Information Engineering, Tianjin University. His current research interests include operation and planning of active distribution networks, modeling, and transient simulation of power systems. Prof. Li is an Associate Editor of IEEE Transactions on Sustainable Energy, CSEE Journal of Power and Energy Systems, Sustainable Energy Technologies and Assessments, and IET Renewable Power Generation.

Hao Yu (Senior Member, IEEE) received the B.S. and Ph.D. degrees in the electrical engineering from Tianjin University, Tianjin, China, in 2010 and 2015, respectively.

He is currently an Associate Professor with the School of Electrical and Information Engineering, Tianjin University, Tianjin, China. His current research interests include the operation analysis and optimization of active distribution networks and integrated energy systems. He is the assistant editor of IET Energy Systems Integration.

Jiancheng Yu is currently with the State Grid Tianjin Electric Power Company, Tianjin, China. His research interests include integrated energy, demand response, and smart power distribution and consumption.

Jinli Zhao (Member, IEEE) received the Ph.D. degree in electrical engineering from Tianjin University, Tianjin, China, in 2007.

She is currently an Associate Professor in the School of Electrical and Information Engineering, Tianjin University. Her research interests include operation and planning of active distribution networks, and power system security and stability.

Guanyu Song (Senior Member, IEEE) received the B.S. and Ph.D. degrees in electrical engineering from Tianjin University, Tianjin, China, in 2012 and 2017, respectively.

He is currently a Senior Engineer with the School of Electrical and Information Engineering, Tianjin University. His current research interests include distributed generation systems, optimal planning, and operation of smart distribution systems.

Jianzhong Wu (Fellow, IEEE) received the B.Sc., M.Sc., and Ph.D. degrees in electrical engineering from Tianjin University, China, in 1999, 2002 and 2004, respectively.

From 2004 to 2006, he was at Tianjin University, where he was an Associate Professor. From 2006 to 2008, he was a Research Fellow at the University of Manchester, Manchester, U.K. He is a Professor of Multi-Vector Energy Systems and the Head of the School of Engineering, Cardiff University, U.K. He is Co-Editor-in Chief of Applied Energy. He is the Co-Director of U.K. Energy Research Centre and EPSRC Supergen Energy Networks Hub. His research interests include integrated multi-energy infrastructure and smart grid.

Chengshan Wang (Senior Member, IEEE) received the Ph.D. degree in electrical engineering from Tianjin University, Tianjin, China, in 1991.

He is currently a Professor with the School of Electrical and Information Engineering, Tianjin University. Prof. Wang is a Member of Chinese Academy of Engineering. His research interests include distribution system analysis and planning, distributed generation system and microgrid. Prof. Wang is the Editor-in-Chief of IET Energy Systems Integration. He is the Director of the Key Laboratory of Smart Grid of Ministry of Education, Tianjin University, Tianjin, China.